Thermoacoustic molecular tomography with magnetic nanoparticle contrast agents for targeted tumor detection

Liming Nie, Zhongmin Ou, Sihua Yang, and Da Xing[a)]
MOE Key Laboratory of Laser Life Science and Institute of Laser Life Science, South China Normal University, Guangzhou 510631, China and College of Biophotonics, South China Normal University, Guangzhou 510631, China

(Received 13 November 2009; revised 30 June 2010; accepted for publication 30 June 2010; published 21 July 2010)

Purpose: The primary feasibility steps of demonstrating the ability of microwave-induced thermoacoustic (TA) in phantoms have been previously reported. However, none were shown to target a diseased site in living subjects in thermoacoustic tomography (TAT) field so far. To determine the expressions of oncogenic surface molecules, it is quite necessary to image tumor lesions and acquire pathogenic status on them via TAT.

Methods: Compared to biological tissues, iron oxide nanoparticles have a much higher microwave absorbance. Fe_3O_4/polyaniline (PANI) nanoparticles were prepared via polymerization of aniline in the Fe_3O_4 superparamagnetic fluids. Then Fe_3O_4/PANI was conjugated to folic acid (FA), which can bind specifically to the surface of the folate receptor used as a tumor marker. FA-Fe_3O_4/PANI targeted tumor was irradiated by pulsed microwave at 6 GHz for thermoacoustic detection and imaging.

Results: The effect of the Fe_3O_4/PANI superparamagnetic nanoparticles for enhancing TAT images was successfully investigated in *ex vivo* human blood and *in vivo* mouse tail. Intravenous administration of the targeted nanoparticles to mice bearing tumors showed fivefold greater thermoacoustic signal and much longer elimination time than that of mice injected with nontargeted nanoparticles in the tumor. The specific targeting ability of FA-Fe_3O_4/PANI to tumor was also verified on fluorescence microscopy.

Conclusions: Fabricated iron oxide nanoparticles conjugated with tumor ligands for targeted TAT tumor detection at the molecular level was reported for the first time. The results indicate that thermoacoustic molecular imaging with functionalized iron oxide nanoparticles may contribute to targeted and functional early cancer imaging. Also, the modified iron oxide nanoparticles combined with suitable tumor markers may also be used as novel nanomaterials for targeted and guided cancer thermal therapy.
[DOI: 10.1118/1.3466696]

Key words: thermoacoustic molecular tomography, folate-functionalized superparamagnetic nanoparticles, folate receptor tumor markers, targeted tumor imaging

I. INTRODUCTION

Microwave-induced thermoacoustic tomography (TAT), which is a hybrid of microwave imaging and ultrasound imaging, integrates rich microwave contrast and good ultrasound resolution in one imaging modality. Thermoacoustic (TA) effect is based on the thermoelastic expansion mechanism after pulsed microwave absorption. Submicrosecond microwave pulse is usually employed to irradiate the tissue; the local heat absorbed by the irradiated tissue depends on the tissue absorption coefficient. Then the absorbed heat would be converted into thermoacoustic waves; thermoacoustic signals can be efficiently generated under the conditions of thermal and stress confinement.[1–3] Within the vaporization threshold of the microwave energy employed, the signal amplitude is in linear relationship with the microwave energy absorption.[4] Moreover, the Grüneisen parameter determines the conversion efficiency of microwave energy deposition to thermoacoustic pressure.[2] These thermoacoustic signals can be acquired by ultrasound transducer and processed for TAT imaging reconstruction.

The recent surge of interest has significantly expanded the depth of photoacoustic (PA) and TAT techniques in biomedical imaging application, such as breast cancer imaging, brain structural and functional imaging, foreign body detection, deep tumor imaging, and recently for molecular imaging.[5–10] The main difference between these two techniques is the contrast mechanism. Hemoglobin and melanin contribute to the main optical absorption in photoacoustic tomography, while ion and water concentration is responsible for TAT contrast. Currently, substantial attention in many imaging methods has been devoted to developing contrast agents not only for improving the contrast of the acquired images but also for molecular imaging, targeting specific biomolecules, gene expression, etc.[11,12]

Superparamagnetic nanoparticles like iron oxides possess unique magnetic properties such as high relaxivity, making them an attractive platform for magnetic resonance imaging. They have been used as contrast agents and drug carriers for detection, diagnosis, and treatment of illnesses such as cancer, cardiovascular disease, and neurological disease.[13–15] Magnetic fluid hyperthermia is another important application for cancer therapy. The superparamagnetic particles can transform the energy of the electromagnetic field into heat due to the hysteresis loss. After conjugating the particles with specific molecules such as antibodies, specific ligands, thiol functional groups, or therapeutic drugs, the functionalized Fe_3O_4 (thermoseeds) can increase the temperature in tumors and therefore kill tumor cells without damaging the surrounding healthy tissues.[16,17]

Initial feasibility steps of contrast agents for TAT have been suggested previously such as single-walled nanotubes or microbubbles used in simulated phantom.[18–20] However, none were shown to target a diseased site in living subjects using TAT so far. The aim of targeting tumor site is to determine the expressions of oncogenic surface molecules, and it is quite necessary to image tumor lesions and acquire pathogenic status on them. Here, we report on fabricated iron oxide nanoparticles conjugated with tumor ligand for targeted TAT tumor detection at the molecular level for the first time. Magnetic Fe_3O_4/polyaniline (PANI) nanoparticles were prepared via polymerization of aniline and then the water-soluble Fe_3O_4/PANI was conjugated to folic acid (FA). The thermoacoustic enhancement effects of the contrast agents were investigated on phantoms and living mouse. Most importantly, the high affinity and specificity of the contrast agents as molecular probe to tumor cells were observed on TAT results and validated on fluorescence microscopy. Therefore, thermoacoustic molecular and functional imaging with folate-functionalized magnetic iron oxide nanoparticles may contribute to early cancer diagnostics and guided hyperthermia in living subjects.

II. MATERIALS AND METHODS

II.A. Chemicals and reagents

The major agents and fluorescent probes used in our research are Fe_3O_4/PANI magnetic composite nanoparticles supplied by State Key Laboratory of Chemical Resource Engineering in Beijing University of Chemical Technology; folic acid, fluorescein isothiocyanate (FITC), dimethyl sulfoxide (DMSO), *N*-hydroxysulfonosuccinimide (NHS), and 1-ethyl-3-(3-(dimethylamino)-propyl) carbodiimide (EDC) were purchased from Sigma-Aldrich (St. Louis, MO). Since all the reagents were of analytical grade, they were used without further purification.

II.B. FA-Fe_3O_4/PANI synthesis

Briefly, the synthesis of Fe_3O_4 cores follows a precipitation method.[21,22] $FeCl_2 \cdot 4H_2O$ and $FeCl_3 \cdot 6H_2O$ were used as iron sources and NaOH was used as a precipitator. Dodecylbenzene sulfonic acid sodium salt (NaDS) was used as a surfactant to prevent agglomeration between the nanoparticles. The precipitates were separated by magnetic decantation with acetone and pure water after cooling the suspension at room temperature. Coating of metallic oxide nanoparticles with PANIs has mostly been studied by several approaches.[23–25] The Fe_3O_4/PANI nanoparticles with core-shell structure were synthesized via an *in situ* polymerization of aniline monomer in an aqueous solution, which contains well-dispersed Fe_3O_4 nanoparticles and NaDS as surfactant and dopant. Fe_3O_4 is the magnetic core, these particles are polydisperse and some of them agglomerated due to magnetodipole interactions between particles; the Fe_3O_4 particles are almost spherical with diameters ranging from 10 to 30 nm. Also PANI is the aqueous and conducting shell and can be easily conjugated to biomarkers, the Fe_3O_4/PANI particles are almost spherical with diameters ranging from 30 to 50 nm.[23–26]

To synthesize Fe_3O_4/PANI with the ability to recognize tumor cells, we chose the folate receptor (FR) as a tumor marker. FR is a highly selective tumor receptor overexpressed in cancer cell membranes and shows considerable promise as a monitoring and therapeutic target for a large number of important human pathologies.[27,28] FA is served as a tumor-homing molecule in this study that can guide Fe_3O_4/PANI into FR-overexpressed tumor cells, which could be applied in the diagnosis for positioning the tumor cells and further treatment. FA (1 mg/ml) was dissolved in DMSO and activated by EDC/NHS to afford FA-NHS (molar ratio, $FA:EDC:NHS=1:1:1$). Fe_3O_4/PANI was mixed with FA-NHS and incubated avoiding light exposure for 12 h. The resulting product, FA-Fe_3O_4/PANI, was dialyzed against phosphate-buffered saline (PBS) by using 1000 Da filter (Millipore) to remove free FA, EDC/NHS, and FA-NHS.

II.C. Cell lines and the animal model

S180 mouse sarcoma tumor cell lines (from Guangzhou Medical College) were cultured under standard conditions. The S180 tumor models were generated by subcutaneous injection of 5×10^7 cells in 50 μl PBS into the flank region of the female Balb/c mice (35–45 g bodyweight). *In vivo* tumor experiments were performed 2 weeks after tumor inoculation on the mice back. The Fe_3O_4/PANI was intravenously injected into the tumor-free mice tail for the TAT molecular imaging experiments at a dose of 150 μl with a concentration of 0.1 mg/ml. For the targeted molecular TAT imaging, two groups of mice bearing S180 sarcoma tumor xenografts with similar morphology were used in the experiment. Each group contains three mice, the two groups were successively injected through the tail vein with either 300 μl of Fe_3O_4/PANI or FA-Fe_3O_4/PANI at a concentration of 0.2 mg/ml. Thermoacoustic images of the tumors and their surrounding tissues were acquired before and up to 5 h after injection. All the mice survived the 2-month observation period after thermoacoustic imaging experiments.

II.D. Fluorescence microscopy of targeted Fe_3O_4/PANI

Fe_3O_4/PANI conjugation was labeled with FITC for the fluorescence microscopy assay.[29,30] To take

FA-Fe_3O_4/PANI-FITC as an example, FITC was first dissolved in DMSO (1 mg/ml). FITC and FA-NHS were mixed with Fe_3O_4/PANI (volume ratio, FITC:FA-NHS:Fe_3O_4/PANI=1:1:1) and incubated for 12 h in the dark. The resulting products were dialyzed against PBS by using 1000 Da filter (Millipore) to remove free FITC and FA-NHS. The preparation of Fe_3O_4/PANI-FITC was similar to the synthesis of FA-Fe_3O_4/PANI-FITC mentioned above.

FITC fluorescence from the tumor was *in vivo* measured on the stage of a stereomicroscope (Lumar V12, Zeiss, Jena, Germany) with a hydrargyrum lamp (HBO100) as the light source. 300 μl PBS, 300 μl Fe_3O_4/PANI-FITC, or FA-Fe_3O_4/PANI-FITC at a concentration of 0.2 mg/ml was directly injected into the tumors; 6 h later, the mice were anesthetized with pentobarbital sodium and were restrained in a specially designed holder for imaging analysis. The magnification is adjusted eightfold for the stereomicroscope observation. The light beam through a 470/40 nm bandpass filter, whose light exposure time could be adjusted automatically for fluorescent images, was used to excite the fluorescent probes. The fluorescent emission was recorded through the 525/50 nm bandpass channel. In addition, the laser beam was blocked by a computer-controlled shutter during the translation of excitation laser wavelength to reduce laser bleaching of FITC and laser exposure of the tissue.

II.E. Data acquisition system and imaging reconstruction

The data acquisition system for TAT molecular imaging mainly composes of B-mode digital ultrasound diagnostic equipment (model CTS-5000B, SIUI, China) with a multielement transducer (L2L50A) and a high speed digital card (PCI-6541, NI, USA). The 128-element linear transducer with a scanning width of 53 mm was used for thermoacoustic signal acquisition. The multielement transducer has a center frequency of 2.5 MHz with a nominal bandwidth of 70%. The transducer array with a computed tomography capability selects and receives the thermoacoustic signals, which are parallel to its center cross section in a limited view.[31] The digital data acquisition (DAQ) card featured a 12-bit analog-to-digital (D/A) converter with a sampling rate of 25 MHz was employed for collecting digital signals. A microwave generator at 6 GHz (BW-6000HPT, China) transmitted out short microwave pulses adjustable from 0.3 to 1.2 μs, whose maximum trigger repetition rate can reach 500 Hz. The microwave pulses were coupled into a rectangular waveguide in the TE_{10} mode with a cross section of $34.8 \times 15.8\ \text{mm}^2$. For 6 GHz microwaves, the penetration depths of fat and muscle are 5.2 and 0.7 cm, respectively.[32] Other soft tissues have a penetration depth between those of fat and muscle. The energy density per volume of the microwave pulse is about $0.25\ \text{mJ/cm}^3$, and the temperature rise is approximately 0.04 mK, according to the previous calculation,[6] which is within the safety standard for animal and human use.[33,34]

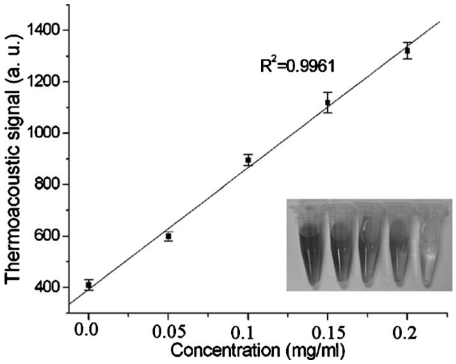

FIG. 1. Linear fitting of thermoacoustic signals of the contrast agents at different concentrations; the solid line is a linear fit with standard deviations ($n=3$). Fe_3O_4/PANIs at different concentrations are shown in the Eppendorf tubes from left to right in the actual inset picture of Fig. 1. The thermoacoustic signal produced by Fe_3O_4/PANIs was observed to be linearly dependent on the concentration ($R^2=0.9961$).

A custom-built control circuit provided a synchronized clock signal to trigger the DAQ card and the microwave generator simultaneously. The TA signals received by the transducer array, after preamplification and phase adjustment, were acquired with the DAQ card and then transferred into a personal computer for subsequent data processing. The mouse in the animal holder can be rotated at several scanning positions for acquisition of multiple image signals with comprehensive tissue information. Generally, the signals at 20 circular scanning positions around the object were sufficient to recover a clear and accurate image. More technical information about the fast signal acquisition system can be found in the previous literature.[31,33,35] Due to the directivity properties of the linear transducer array, an improved limited-field-filtered backprojection algorithm is employed for the TAT image formation.[6,36]

III. RESULTS

III.A. Functionalized iron oxide nanoparticles for TAT molecular imaging

A stable water-soluble Fe_3O_4/PANI suspension was obtained after the final centrifugation of the solution. In a phantom study, TA signals of Fe_3O_4/PANIs at different concentrations, as shown in the Eppendorf tubes from left to right in the actual inset picture, are detected under the same microwave energy density. It can be seen that the TA signal produced by Fe_3O_4/PANI solution is in linear relationship with their concentrations ($R^2=0.9961$) in Fig. 1. These data suggest that the TA signal of the contrast agent is much higher than that of water, and Fe_3O_4/PANI solution at a concentration of 0.1 mg/ml can achieve effective signal increase.

Different concentrations of Fe_3O_4/PANI solution mixed with human blood were also investigated to estimate the appropriate concentration for TAT molecular imaging. Three identical plastic tubes with a diameter of 0.8 mm filled with human blood and Fe_3O_4/PANI solution were embedded at a depth of 10 mm in porky fat tissue, the cross section of the three tubes' placement is shown in the inset picture of Fig.

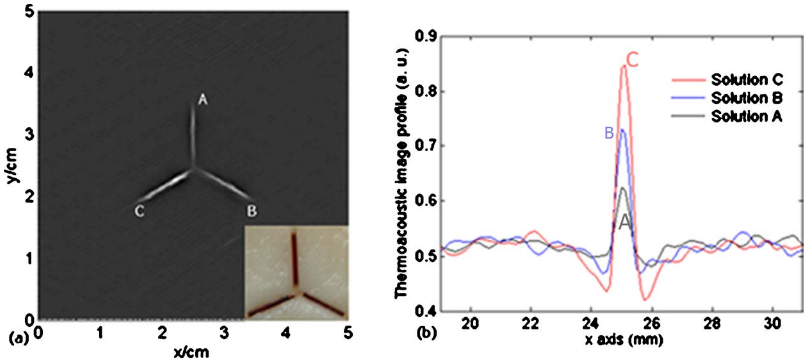

FIG. 2. (a) Thermoacoustic imaging of thermoacoustic contrast agents mixed with human blood at three different concentrations in plastic tubes. (b) The corresponding profiles of the thermoacoustic signals through the center of the three tubes for quantitative analysis.

2(a). The tube marked "A" was filled with 300 μl pure blood, another one marked "B" was filled with 150 μl Fe_3O_4/PANI solution of 0.05 mg/ml mixed with 150 μl blood; and the other one was filled with 150 μl Fe_3O_4/PANIs of 0.1 mg/ml with 150 μl blood.

The TAT image in Fig. 2(a) obtained by circular scanning at 20 scanning positions agrees well with the actual phantom shown in the inset of Fig. 2(a).[31,3] Signal-noise-ratio (SNR) is defined as the ratio of TAT signal amplitude from the imaging object to the background noise amplitude corrupting the signal; a high-contrast TAT image can be reconstructed using signals with high SNR. The thermoacoustic map of tube "C" containing Fe_3O_4/PANIs and blood has a much higher SNR than that of tube A containing blood only due to high microwave absorption of the exogenous contrast agent. Reconstructed profiles of the three tubes were chosen vertically across the tube midpoint. According to quantitative analysis, as shown in Fig. 2(b), the TA signal SNR can be increased roughly four times using a Fe_3O_4/PANI enhanced sample compared to pure blood.

III.B. *In vivo* TA imaging of Fe_3O_4/PANIs in mouse tail

The phantom experiment was initially tested as a precursor to warrant the potential *in vivo* experiments. First, the great enhancement effect of the contrast agents on the thermoacoustic signal was corroborated by tissue mimicking phantom imaging studies. Second, the pilot reference concentration at the level of 0.1 mg/ml needs further corroboration on the *in vivo* study. In living subjects, the contrast agents may be diluted by the blood circulation system. Therefore, the enhancement of the contrast agents on living subject may be smaller than that on phantom with identical concentration. In order to investigate the enhancement effect of the contrast agents on living subjects, the microwave energy used for generating ultrasound signals was quite moderate at 0.2 mJ/cm^3. The microwave generator works synchronously with the sampling card at a frequency of 10 Hz (10 pulses/s). Image acquisition of the mouse tail began approximately 120 min following administration. The signals at one scanning position were employed to reconstruct TAT image.

Two thermoacoustic angiographs of the mouse tail are presented in Figs. 3(a) and 3(b). The experiments were performed in a vertical data acquisition mode, as depicted in Fig. 3(c); the signal receiving plane of the linear transducer array is vertical to the microwave illumination direction. The anesthetized mouse was placed in an animal holder and then protruded into the tank under a piece of clear thin membrane. The tank was filled with mineral oil to couple the induced thermoacoustic waves to the transducer array. The brightly visible thermoacoustic image of the mouse tail after injection of Fe_3O_4/PANI contrast agent [Fig. 3(b)] shows three times greater contrast enhancement than the control image without any contrast agent [Fig. 3(a)]. The contrast agent nanoparticles left in animal subject also contribute a lot to TAT signal enhancement despite the blood stream circulation. This experiment successfully demonstrated the feasibility of using our TA molecular imaging system to image Fe_3O_4/PANIs *in vivo*.

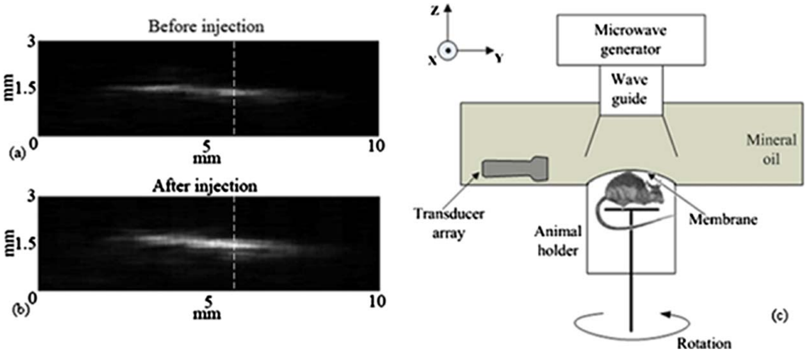

FIG. 3. *In vivo* thermoacoustic imaging of the mouse tail before and after intravenous injection of the contrast agent suspension. (a) Control TA image of the mouse tail without Fe_3O_4/PANI injection. (b) TA image of the mouse tail after Fe_3O_4/PANI injection. (c) Schematic of TA molecular tomography system.

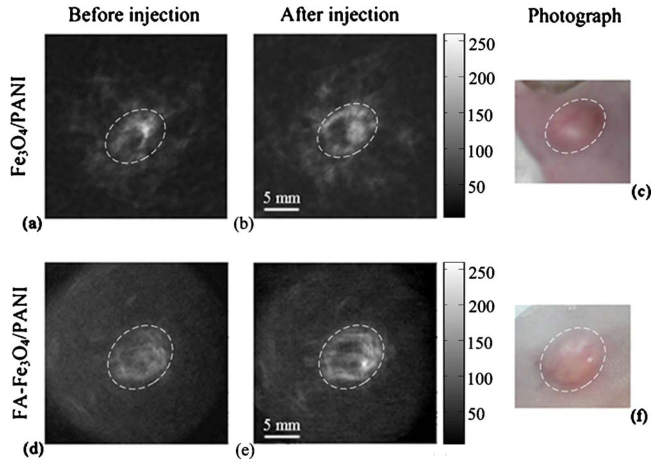

FIG. 4. *In vivo* thermoacoustic imaging of tumors with contrast agent bearing in mouse. [(a) and (d)] TAT images of control sample injected with PBS. [(b) and (e)] TAT images of tumor injected with Fe_3O_4/PANI and Fe_3O_4/PANI-FA, respectively. [(c) and (f)] Photographs of tumor's area on the mouse back.

III.C. TAT molecular imaging with selective targeting on tumor model

To give quantitative analysis to the image enhancement by the contrast agents, a region of interest in the white dashed line around the tumor was selected in all the thermoacoustic images. Thermoacoustic signals were calculated in the tumors whose boundaries were clearly visualized in the ellipses. Specifically, thermoacoustic images of one mouse from each group before and 4 h after injection were displayed in Fig. 4. The images in the first row represent the control mice group injected with nontargeted contrast agents, while the second row represents another mice group injected with targeted contrast agents. In the mice without any contrast agents, the thermoacoustic signal, likely produced by the tumor absorption, was seen in the preinjection images [Figs. 4(a) and 4(d)] with its actual picture shown in Figs. 4(c) and 4(f). The mouse sarcoma tumor, which highly expresses FR biomarkers, was clearly exhibited by thermoacoustic molecular image, as shown in Fig. 4(e).

In the reconstructed thermoacoustic images [Figs. 4(a), 4(b), 4(d), and 4(e)] of the tumor model, outer bright rings in the thermoacoustic images represent the boundary between the tumor and the normal tissue corresponding to the cancer invasion front with rapid cell proliferation and robust angiogenesis in the tumor.[37,38] A small increase in ionic conductivity or water content can produce a significant increase in microwave absorption at the margin of the tumor. Ring patterns have also been reported in photoacoustic imaging with rim enhancement correlating well with ratios of tumor periphery-core microvessel densities.[39] The TAT modality is generally better suited at delineating tumor edges at the location of the contrast and may supply complementary information for other existing imaging modalities.[40,41]

A subtraction image was calculated in the ellipses between the thermoacoustic image acquired postinjection and the thermoacoustic image acquired before injection. Each thermoacoustic signal increment was a statistical result of three mice; standard deviations are shown as symbol in Fig. 5. The thermoacoustic increment was quantified as a function of time. The above plot represents the subtraction of the thermoacoustic signals obtained on mice injected with targeted contrast agents, whereas the below plot represents the subtraction traction of the thermoacoustic signals obtained on mice injected with nontargeted contrast agents. It can be seen in Fig. 5 that plain Fe_3O_4/PANIs led only to a temporary increase in the thermoacoustic signal of the tumor with a sharp decreasing trend after several hours, while FA-Fe_3O_4/PANI led to a consistently higher thermoacoustic signal. On average, the targeted nanoparticles can lead to fivefold greater thermoacoustic signal than mice injected with nontargeted nanoparticles in the tumor.

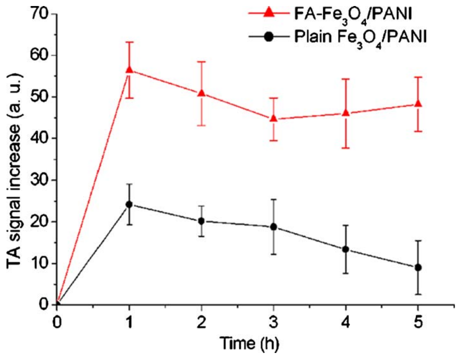

FIG. 5. Thermoacoustic signals of tumor injected with contrast agents at different times. Thermoacoustic signals were calculated in the tumors whose boundaries were clearly visualized in the dashed ellipses, the thermoacoustic enhancement can be steadily strengthened by the targeted contrast agents compared to nontargeted contrast agents. The mean TA signal in the tumor region of interest was calculated for each TAT image ($n=3$); the error bars represent standard error.

III.D. Fluorescence verification of FA-Fe_3O_4/PANI targeting ability

The targeting ability of the functionalized magnetic nanoparticles to tumor was validated on a fluorescence microscopy as an independent method in Fig. 6. The images in the first row correspond to control tumor tissue injected with PBS, the middle row corresponds to another tumor model injected with Fe_3O_4/PANI-FITC, while the bottom row corresponds to the other tumor model injected with FA-Fe_3O_4/PANI-FITC. Similarly, the images in the left column correspond to fluorescent images under white light the middle column corresponds to fluorescent emission, and the right column corresponds to the overlaid fluorescent image by combining the left and middle images.

The mouse fur surrounding the tumor was shaved and chemically depilated before experiments, and the skin above the tumor xenograft was very thin and a little transparent. Although the fluorescence cannot penetrate very deeply into the tumor, the shallow layer of the tumor stuck to the skin can be imaged. The bright fluorescent image in the second row compared to the dark fluorescent image in the first row can verify the penetration ability of fluorescence. The tumors

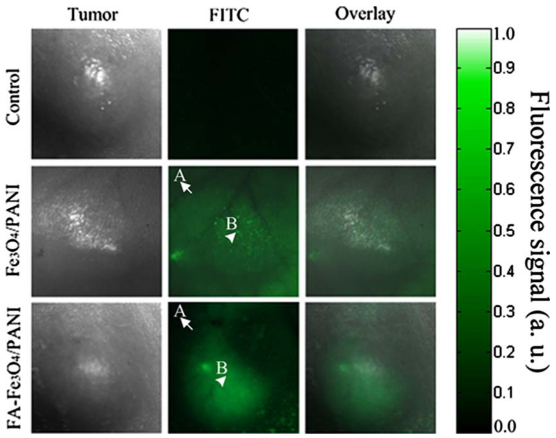

FIG. 6. Fluorescence histological imaging of tumor and normal tissue 6 h after injection of contrast agents, observed with a fluorescence stereomicroscope. The first row corresponds to control tumor tissue injected with PBS, the middle row corresponds to another tumor model injected with Fe_3O_4/PANI-FITC, while the bottom row corresponds to tumor model injected with FA-Fe_3O_4/PANI-FITC. The left column corresponds to fluorescent images under white light, the middle column corresponds to fluorescent emission under laser excitation on 470/40 nm, and the right column corresponds to the overlaid fluorescent image by combining the left and middle images.

contained much more contrast agents than the vasculature because of the direct injection of contrast agents into the tumors and the bloodstream clear. Therefore, FA-Fe_3O_4/PANI-FITC specifically bound to the tumor receptors would lead to a brilliant fluorescent signal, whereas vasculature containing less FITC conjugates would result in dark shadow appearance, as shown in the fluorescent images.

For quantitative analysis, the arrow marked A refers to the fluorescence on the normal tissue with a fixed distance outside the tumor center, while the arrowhead marked B refers to the fluorescence at the tumor center. The ratio of B to A can be used as an indicator for the contrast agent targeting ability. The fluorescence of FA-Fe_3O_4/PANI was detected inside the tumor, but almost not in the normal tissue around the tumors in Fig. 6. (The specific fluorescence values of B and A are 122 and 13, respectively, in the central fluorescence image of the third row.) However, the fluorescence of Fe_3O_4/PANI was detected in both the injected tumor and surrounding normal tissue. (The specific fluorescence values of B and A are 100 and 52, respectively, in the central fluorescent image of the second row.) The normal tissue surrounding the tumor injected with Fe_3O_4/PANI-FITC shows a much more intense fluorescent emission than that surrounding the tumor injected with FA-Fe_3O_4/PANI-FITC (fluorescence value at 52 compared to fluorescence value at 13). The control sample was injected with PBS, no fluorescence was detected on it (the fluorescent values are below 11).

Two more cohorts of mice have been used in the experiment to acquire statistical data. In Fig. 6, the ratio of B to A in the mouse injected with FA-Fe_3O_4/PANI is 9.38 and is much greater than that of B to A in the mouse injected with Fe_3O_4/PANI at 1.92. In another cohort of mice, the corresponding ratios are 16.2 and 1.83, respectively. In the third cohort of mice, the ratios are 22.1 and 1.82, respectively. These statistical numbers ($n=3$) can prove that FA-Fe_3O_4/PANI has a higher selectivity and greater affinity with tumor cells than Fe_3O_4/PANI due to the tumor-specific ligands. This study also shows that the FA-Fe_3O_4/PANI would not accumulate in the tissue surrounding the tumor and Fe_3O_4/PANI alone could easily reach the surrounding tissue through intracellular diffusion.

IV. CONCLUSION AND DISCUSSION

Intravenous injection of targeted Fe_3O_4/PANIs in mice led to almost fivefold higher thermoacoustic signal in the tumor compared to mice injected with nontargeted Fe_3O_4/PANIs on S180 mouse tumor model *in vivo*. The temporary and decreasing thermoacoustic signal observed for plain Fe_3O_4/PANI is likely caused by the clearing of the blood circulation system. In contrast, FA-Fe_3O_4/PANI binds to the tumor angiogenesis receptors,[42] creating a consistent thermoacoustic signal from the tumor. The specificity and selectivity of the targeted magnetic nanoparticles to tumor were verified using florescence microscopy as an independent method. Thus, the contrast between the experimental groups (targeted FA-Fe_3O_4/PANI injection and the control group Fe_3O_4/PANI injection) indicates specific targeting of FA-Fe_3O_4/PANI probe targeted with tumor cells. This study suggests that thermoacoustic molecular imaging with ligand-functionalized Fe_3O_4/PANIs can achieve good contrast enhancement and may be used as specific antibody shuttle for thermoacoustic molecular imaging.

Compared to hydrophobic nanoparticles above 100 nm, the FA-Fe_3O_4/PANI nanoparticles have an increased affinity for molecular targets because of longer retention time.[43,44] Long retention time of FA-conjugated Fe_3O_4/PANI in the tumor markers has major implications for monitoring diagnosis and drug delivery process. Biocompatibility has been an important issue for *in vivo* applications of functionalized iron oxide nanoparticles; the mice in the experiments all survived the 2-month observation period with satisfactory results. Furthermore, TAT overcomes the resolution drawback of pure optics imaging while retaining the most compelling features of both microwave and ultrasound, namely, high microwave absorption contrast and submillimeter ultrasound resolution—up to an imaging depth of several centimeters.[45] Significant folate uptake would also be seen at sites of inflammation because of the FR overexpression on activated macrophages.[46] Therefore, sarcoma cancer cells receptor binding as well as tumor uptake by activated macrophage can contribute to the accumulation of folate conjugates.

Targeting efficiency of the targeted contrast agents to the tumor receptors is affected by several factors and may not be as high as expected. Using higher concentration of contrast agents and higher microwave energy density would result in greater image enhancement and more obvious result. FA-conjugated iron oxide nanoparticles may have better targeting efficiency and signal enhancement on tumors with small size because the nanoparticles could accumulate in a limited volume (smaller tumor size) with a much higher distribution density. Tumor at good physiological condition such as at early angiogenesis stage usually has fast metabolism speed, thus more nanoparticles would be taken up and contribute to greater enhancement effect in the tumor. The extravasation ability of the particles exiting vasculature would also influence the targeting efficiency to the cancer cells.[10] Different animal and different tumors may cause change in the TAT signal; the targeting mechanism needs more future further studies. We also expect this work to stimulate further studies of biologically relevant problems in thermoacoustic molecular imaging.

The sensitivity of our TAT molecular imaging system to the iron oxide nanoparticles is not very high. The detection sensitivity can be improved by increasing the incident microwave energy density toward the maximum permissible exposure, choosing optimal detection bandwidth, detection electronics, and so on. Small sample size in the experiments may lead to measurement error because of individual differences, and experimental results on a bigger sample size would be more compelling and make the experimental results more accurate. This study demonstrated a pilot feasibility study for targeted cancer imaging on TAT, which is suggestive and indicative for TAT field and targeted molecular imaging. However, *in vivo* demonstration of targeting needs to be verified more accurately and maybe through standard methods such as histology, mass spectroscopy, *etc.*, which is our next work in the near future.

The microwave generator employed in our laboratory has a maximum repetition frequency of 500 Hz, which is high enough for the magnetic particles to elevate the temperature of the irradiated tumors in a short time. The functionalized particles can specifically target the corresponding tumor and effectively enhance the thermal destruction of tumor cells without damaging the nontargeted normal tissue. On the other hand, the TA signal amplitude of the irradiated tissue is in linear correlation with its temperature, according to recent literature.[4,47] When the microwave pulse heats up the tumor tissue, it would also trigger out thermoacoustic signals. Thus, TAT can monitor and guide the hyperthermia effect at the same time of thermal treatment using one microwave generator. Therefore, functionalized iron oxide combined with suitable tumor markers may be used as novel nanomaterials for targeted cancer thermal therapy.

ACKNOWLEDGMENTS

This research was supported by the National Basic Research Program of China (Grant No. 2010CB732602), the Program for Changjiang Scholars and Innovative Research Team in University (Grant No. IRT0829), the National Natural Science Foundation of China (Grant Nos. 30627003, 30870676, and 30800261), the Natural Science Foundation of Guangdong Province (Grant No. 7117865), and the Scientific Research Foundation of the State Human Resource Ministry for Returned Chinese Scholars (2008). The authors also acknowledge Professor Donglin Zhao for the supply of Fe_3O_4/PANI nanoparticles and Dr. Feifan Zhou for the helpful discussion.

[a] Author to whom correspondence should be addressed. Electronic mail: xingda@scnu.edu.cn; Telephone: +86-20-8521-0089; Fax: +86-20-8521-6052.

[1] T. Bowen, "Radiation-induced thermoacoustic imaging," US Patent No. 4,385,634 (1983).

[2] L. V. Wang, "Multiscale photoacoustic microscopy and computed tomography," Nat. Photonics **3**(9), 503–509 (2009).

[3] R. A. Kruger, W. L. Kiser, Jr., D. R. Reinecke, and G. A. Kruger, "Thermoacoustic computed tomography using a conventional linear transducer array," Med. Phys. **30**, 856–860 (2003).

[4] M. Pramanik and L. V. Wang, "Thermoacoustic and photoacoustic sensing of temperature," J. Biomed. Opt. **14**(5), 054024 (2009).

[5] R. A. Kruger, K. D. Miller, H. E. Reynolds, W. L. Kiser, D. R. Reinecke, and G. A. Kruger, "Breast cancer *in vivo* contrast enhancement with thermoacoustic CT at 434 MHz—Feasibility study," Radiology **216**, 279–283 (2000).

[6] L. Nie *et al.*, "Microwave-induced thermoacoustic scanning CT for high-contrast and noninvasive breast cancer imaging," Med. Phys. **35**(9), 4026–4032 (2008).

[7] X. Wang *et al.*, "Noninvasive laser-induced photoacoustic tomography for structural and functional in vivo imaging of the brain," Nat. Biotechnol. **21**, 803–806 (2003).

[8] L. Nie, D. Xing, D. W. Yang, L. M. Zeng, and Q. Zhou, "Detection of foreign body using fast thermoacoustic tomography with a multielement linear transducer array," Appl. Phys. Lett. **90**, 174109 (2007).

[9] J. A. Copland *et al.*, "Bioconjugated gold nanoparticles as a molecular based contrast agent: Implications for imaging of deep tumors using optoacoustic tomography," Mol. Imaging Biol. **6**(5), 341–349 (2004).

[10] A. De La Zerda *et al.*, "Carbon nanotubes as photoacoustic molecular imaging agents in living mice," Nat. Nanotechnol. **3**, 557–562 (2008).

[11] D. Razansky *et al.*, "Multispectral opto-acoustic tomography of deep-seated fluorescent proteins *in vivo*," Nat. Photonics **3**, 412–417 (2009).

[12] L. Li, R. Zemp, G. Lungu, G. Stoica, and L. V. Wang, "Photoacoustic imaging of lacZ gene expression in vivo," J. Biomed. Opt. **12**(2), 020504 (2007).

[13] L. de Rochefort *et al.*, "*In vivo* quantification of contrast agent concentration using the induced magnetic field for time-resolved arterial input function measurement with MRI," Med. Phys. **35**(12), 5328–5339 (2008).

[14] S. A. Wickline, A. M. Neubauer, P. M. Winter, S. D. Caruthers, and G. M. Lanza, "Molecular imaging and therapy of atherosclerosis with targeted nanoparticles," J. Magn. Reson. Imaging **25**, 667–680 (2007).

[15] C. Corot *et al.*, "Macrophage imaging in central nervous system and in carotid atherosclerotic plaque using ultrasmall superparamagnetic iron oxide in magnetic resonance imaging," Invest. Radiol. **39**, 619–625 (2004).

[16] P. Moroz, S. K. Jones, and B. N. Gray, "Magnetically mediated hyperthermia: Current status and future directions," Int. J. Hyperthermia **18**, 267–284 (2002).

[17] J. B. Weaver, A. M. Rauwerdink, and E. W. Hansen, "Magnetic nanoparticle temperature estimation," Med. Phys. **36**(5), 1822–1829 (2009).

[18] X. Jin *et al.*, "Iron oxide nanoparticles as a contrast agent in thermoacoustic tomography," Proc. SPIE **6437**, 64370E–1-7 (2007).

[19] M. Pramanik *et al.*, "Single-walled carbon nanotubes as a multimodal thermoacoustic and photoacoustic contrast agent," J. Biomed. Opt. **14**(3), 034018 (2009).

[20] A. Mashal, J. H. Booske, and S. C. Hagness, "Toward contrast-enhanced microwave-induced thermoacoustic imaging of breast cancer: An experimental study of the effects of microbubbles on simple thermoacoustic targets," Phys. Med. Biol. **54**, 641–650 (2009).

[21] J. Gupta and M. Gupta, "Synthesis and surface engineering of iron oxide nanoparticles for biomedical applications," Biomaterials **26**, 3995–4021 (2005).

[22] S. Laurent *et al.*, "Magnetic iron oxide nanoparticles: Synthesis, stabilization, vectorization, physicochemical characterizations, and biological applications," Chem. Rev. (Washington, D.C.) **108**, 2064–2110 (2008).

[23] D. Zhao *et al.*, "Inductive heat property of Fe_3O_4/polymer composite nanoparticles in an ac magnetic field for localized hyperthermia," Biomed. Mater. **1**(3), 198–201 (2006).

[24] S. Pal and E. C. Alocilja, "Electrically active polyaniline coated magnetic (EAPM) nanoparticle as novel transducer in biosensor for detection of Bacillus anthracis spores in food samples," Biosens. Bioelectron. **24**, 1437–1444 (2009).

[25] J. Deng *et al.*, "Magnetic and conductive Fe_3O_4-polyaniline nanoparticles

with core–shell structure," Synth. Met. **139**, 295–301 (2003).

[26] O. Yavuz *et al.*, "Synthesis and the physical properties of MnZn ferrite and NiMnZn ferrite-polyaniline nanocomposite particles," J. Mater. Chem. **15**, 810–817 (2005).

[27] J. Sudimack and R. J. Lee, "Targeted drug delivery via the folate receptor," Adv. Drug Delivery Rev. **41**, 147–162 (2000).

[28] D. S. Theti, V. Bavetsias, L. A. Skelton, J. Titley, D. Gibbs, G. Jansen, and A. L. Jackman, "Selective delivery of CB300638, a cyclopenta[g]quinazoline-based thymidylate synthase inhibitor into human tumor cell lines overexpressing the a-isoform of the folate receptor," Cancer Res. **63**, 3612–3618 (2003).

[29] G. B. Wisdom, "Conjugation of antibodies to fluorescein or rhodamine," Methods Mol. Biol. **295**, 131–134 (2005).

[30] Zh. Ou *et al.*, "Functional single-walled carbon nanotubes based on an integrin $a_v\beta_3$ monoclonal antibody for highly efficient cancer cell targeting," Nanotechnology **20**, 105102 (2009).

[31] D. W. Yang, D. Xing, S. H. Yang, and L. Z. Xiang, "Fast full-view photoacoustic imaging by combined scanning with a linear transducer array," Opt. Express **15**, 15566–15575 (2007).

[32] C. C. Johnson and A. W. Guy, "Nonionizing electromagnetic wave effects in biological materials and systems," Proc. IEEE **60**, 692–718 (1972).

[33] L. Nie *et al.*, "*In vivo* detection and imaging of low-density foreign body with microwave-induced thermoacoustic tomography," Med. Phys. **36**(8), 3429–3437 (2009).

[34] IEEE Standard for Safety Levels with Respect to Human Exposure to Radio Frequency Electromagnetic Fields 3 kHz to 300 GHz, IEEE Std. C95.1, 2005.

[35] Y. Zeng, D. Xing, Y. Wang, B. Yin, and Q. Chen, "Photoacoustic and ultrasonic coimage with a linear transducer array," Opt. Lett. **29**, 1760–1762 (2004).

[36] D. W. Yang, D. Xing, H. M. Gu, Y. Tan, and L. M. Zeng, "Fast multielement phase-controlled photoacoustic imaging based on limited-field-filtered back-projection algorithm," Appl. Phys. Lett. **87**, 194101 (2005).

[37] T. P. Padera, B. R. Stoll, J. B. Tooredman, D. Capen, E. Di Tomaso, and R. K. Jain, "Cancer cells compress intratumour vessels," Nature (London) **427**, 695 (2004).

[38] G. D. Yancopoulos, S. Davis, N. W. Gale, J. S. Rudge, S. J. Wiegand, and J. Holash, "Vascular-specific growth factors and blood vessel formation," Nature (London) **407**, 242–248 (2000).

[39] S. Manohar, S. E. Vaartjes, J. C. G. van Hespen, J. M. Klaase, F. M. van den Engh, W. Steenbergen, and T. G. van Leeuwen, "Initial results of in vivo non-invasive cancer imaging in the human breast using near-infrared photoacoustics," Opt. Express **15**, 12277–12285 (2007).

[40] L. S. Bouchard *et al.*, "Picomolar sensitivity MRI and photoacoustic imaging of cobalt nanoparticles," Proc. Natl. Acad. Sci. U.S.A. **106**(11), 4085–4089 (2009).

[41] D. Razansky and V. Ntziachristos, "Hybrid photoacoustic fluorescence molecular tomography using finite-element-based inversion," Med. Phys. **34**(11), 4293–4301 (2007).

[42] S. D. Konda, M. Aref, M. Brechbiel, and E. C. Wiener, "Development of a tumor-targeting MR contrast agent using the high-affinity folate receptor: Work in progress," Invest. Radiol. **35**(1), 50–57 (2000).

[43] R. Weissleder *et al.*, "Cell-specific targeting of nanoparticles by multivalent attachment of small molecules," Nat. Biotechnol. **23**, 1418–1423 (2005).

[44] Zh. Liu, W. B. Cai, L. N. He, N. Nakayama, K. Chen, X. M. Sun, X. Y. Chen, and H. J. Dai, "*In vivo* biodistribution and highly efficient tumour targeting of carbon nanotubes in mice," Nat. Nanotechnol. **2**(1), 47–52 (2007).

[45] H. Jiang, Ch. Li, D. Pearlstone, and L. L. Fajardo, "Ultrasound-guided microwave imaging of breast cancer: Tissue phantom and pilot clinical experiments," Med. Phys. **32**(8), 2528–2535 (2005).

[46] P. S. Low, W. A. Henne, and D. D. Doorneweerd, "Discovery and development of folic-acid-based receptor targeting for imaging and therapy of cancer and inflammatory diseases," Acc. Chem. Res. **41**(1), 120–129 (2008).

[47] I. V. Larina, K. V. Larin, and R. O. Esenaliev, "Real-time optoacoustic monitoring of temperature in tissues," J. Phys. D **38**(15), 2633–2639 (2005).